Inorganic Chemistry

Article

pubs.acs.org/IC

Electron Transfer and Proton-Coupled Electron Transfer Reactivity and Self-Exchange of Synthetic [2Fe−2S] Complexes: Models for Rieske and mitoNEET Clusters

Caroline T. Saouma,[†,‡] Margaux M. Pinney,[†] and James M. Mayer*[,†]

[†]Department of Chemistry, University of Washington, Box 351700, Seattle, Washington 98195-1700, United States

Supporting Information

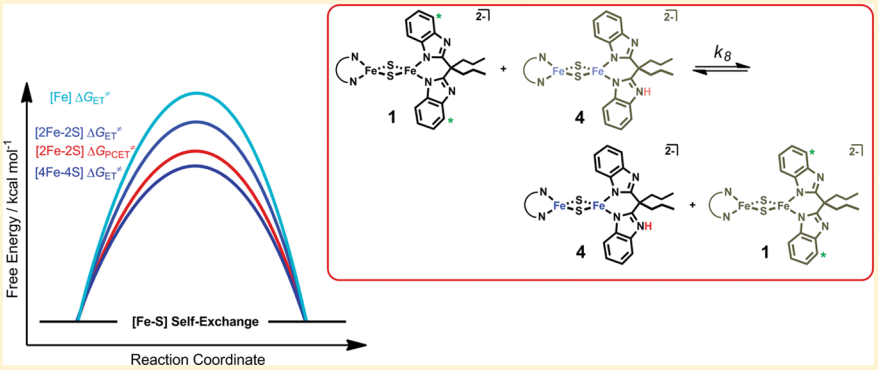

ABSTRACT: This report describes the thermochemistry, proton-coupled electron transfer (PCET) reactions and self-exchange rate constants for a set of bis-benzimidazolate-ligated [2Fe−2S] clusters. These clusters serve as a model for the chemistry of biological Rieske and mitoNEET clusters. PCET from $[Fe_2S_2(^{Pr}bbim)(^{Pr}bbimH)]^{2-}$ (**4**) and $[Fe_2S_2(^{Pr}bbim)(^{Pr}bbimH_2)]^{1-}$ (**5**) to TEMPO occurs via concerted proton−electron transfer (CPET) mechanisms ($^{Pr}bbimH_2$ = 4,4-bis-(benzimidazol-2-yl)heptane). Intermolecular electron transfer (ET) self-exchange between $[Fe_2S_2(^{Pr}bbim)_2]^{2-}$ (**1**) and $[Fe_2S_2(^{Pr}bbim)_2]^{3-}$ (**2**) occurs with a rate constant of $(1.20 \pm 0.06) \times 10^5$ M^{-1} s^{-1} at 26 °C. A similar self-exchange rate constant is found for the related [2Fe−2S] cluster $[Fe_2S_2(SArO)_2]^{2-/3-}$, $SArO^{2-}$ = thiosalicylate. These are roughly an order of magnitude slower than that reported for larger [4Fe−4S] clusters and 1 order of magnitude faster than that reported for N-ligated high-spin iron complexes. These results suggest that the rate of intermolecular ET to/from [Fe−S] clusters is modulated by cluster size. The measured PCET self-exchange rate constant for **1** and **4** at −30 °C is $(3.8 \pm 0.7) \times 10^4$ M^{-1} s^{-1}. Analysis of rate constants using the Marcus cross-relation suggests that this process likely occurs via a concerted proton−electron transfer (CPET) mechanism. The implications of these findings to biological systems are also discussed, including the conclusion that histidine-ligated [2Fe−2S] clusters should not have a strong bias to undergo concerted e^-/H^+ transfers.

I. INTRODUCTION

Iron−sulfur ([Fe−S]) clusters are ubiquitous electron-transfer (ET) cofactors that play a prominent role in many enzymes that mediate multi-e^-/H^+ redox transformations.[1] In some instances, proton transfer (PT) accompanies ET, and the cluster undergoes proton-coupled electron transfer (PCET).[2] As this type of reactivity is increasingly being recognized to prevail in biological [Fe−S] clusters, it is important to establish factors that affect the occurrence and the mechanisms of PCET (stepwise ET-PT or PT-ET, or concerted proton−electron transfer, termed CPET).

Perhaps the most-studied biological [Fe−S] cluster known to mediate PCET is the [2Fe−2S] Rieske cluster, in which one Fe is ligated by two Cys residues, and the other by two His residues.[2a,3] The PCET reactivity enables the Rieske cluster of oxygenase enzymes to serve as both an ET cofactor, delivering electrons to the active site, and a structural gate, with reduction/protonation of the cluster inducing structural changes that affect the active site.[3c] PCET is also the primary function of the Rieske cluster in the Q-cycle of the mitochondrial and photosynthetic electron transport chains.[3b,4] In this latter role, the diferric cluster accepts a net H-atom (e^- + H^+) from a hydroquinone at the b-site. This reduces the cluster to the mixed-valence state and protonates the imidazolate (His) ligand (the resulting semiquinone reduces cytochrome b). The cluster then migrates to the c-site, donating an electron to cytochrome c and the proton to a nearby base. The mechanism of the initial PCET event is debated, with arguments for both stepwise PT-ET[5] and CPET[3a,b] being advanced.[6] Even less is known about both the mechanism and base for the second PCET event. As ET within the Q-cycle is tightly regulated to avoid formation of reactive oxygen species and energetically

Received: December 22, 2013
Published: March 4, 2014

   dx.doi.org/10.1021/ic403131p | Inorg. Chem. 2014, 53, 3153−3161

wasteful short-circuits,[4a,7] it is of interest to understand the mechanism(s) of PCET of Rieske clusters.

In addition to the Rieske cluster, the recently discovered 3-Cys 1-His mitoNEET [2Fe−2S] cluster has also been shown to mediate PCET.[2b] Clusters of this type are found in the outer mitochondrial membrane[8] and are promising targets for cancer and diabetes therapeutics.[2b,9,10] The exact role of mitoNEET clusters remains unknown, and it has been suggested that they serve as a cluster transfer protein[11] and/or play a role in redox reactions,[12] bioenergetics, and redox-sensing.[13] The lone His-residue is crucial in controlling the reduction potential,[14] cluster stability,[12] and PCET.[14] The potential to develop therapeutics, coupled with the uncertainty in its native function, lends further motivation for studies that establish the thermochemical, reactivity, and/or intrinsic properties of His-ligated [Fe−S] clusters.

Herein, we describe detailed thermochemical and kinetic studies of a set of bis-benzimidazolate-ligated [2Fe−2S] clusters, which serve as a model for Rieske and mitoNEET clusters. Our initial report described the synthesis and properties of the clusters and preliminary kinetic studies.[15] We now show that three distinct protonation states can be accessed in the mixed-valence state and hence that PCET can occur from two distinct cluster congeners that differ by a proton. Kinetic analysis and H/D kinetic isotope effects (KIEs) for the PCET reactions with TEMPO are discussed and compared to the measured KIEs of Rieske proteins. Additionally, we examine the self-exchange rate constants for ET, PT, and PCET. These results indicate that the mechanism of PCET at His-ligated [2Fe−2S] clusters should depend primarily on the thermodynamic coupling of the redox partner, and the findings also suggest that the rate of ET at [Fe−S] clusters is influenced by cluster size.

II. RESULTS

II.1. Synthesis and Characterization of Cluster Congeners. The various cluster congeners are shown in Scheme 1. The synthesis and characterization of diferric $[Fe_2S_2(^{Pr}bbim)_2]^{2-}$ (**1**), mixed-valence $[Fe_2S_2(^{Pr}bbim)_2]^{3-}$ (**2**), diferric and protonated $[Fe_2S_2(^{Pr}bbim)(^{Pr}bbimH)]^{-}$ (**3**), and mixed-valence and protonated $[Fe_2S_2(^{Pr}bbim)(^{Pr}bbimH)]^{2-}$ (**4**) are reported elsewhere ($^{Pr}bbimH_2$ = 4,4-bis-(benzimidazol-2-yl)heptane).[15,16]

The mixed-valence and twice-protonated cluster, $[Fe_2S_2(^{Pr}bbim)(^{Pr}bbimH_2)]^{-}$ (**5**), has not been previously characterized, but it was invoked as an electrochemically observed intermediate in cyclic voltammograms (CVs) of **4** at −20 °C (generated in situ from **2** and 1 equiv of [pyH]OTf; py = pyridine).[15] Such CV experiments show two quasi-reversible couples that are anodically shifted relative to the **1**/**2** couple. These are assigned to the **3**/**4** couple and to that of the twice-protonated cluster congeners. Addition of 1 equiv of base regenerates the cyclic voltammogram of **2**, indicating that the doubly protonated mixed-valence **5** might have enough stability at reduced temperatures for generation and characterization.

Indeed, access to **5** is achieved by addition of 2 equiv of [DMAP-H]OTf to MeCN solutions of **2** at −24 °C (DMAP-H^+ = protonated 4-dimethylaminopyridine). Over the course of minutes, solutions of **5** (0.47 mM in MeCN) darken and form solids at room temperature (see Figures S1−S4). Despite this thermal instability, solutions of **5** can be prepared at reduced temperatures for characterization.

Scheme 1. Double Square Scheme for $[Fe_2S_2(^{Pr}bbim)_x(^{Pr}bbimH_y)_{2-x}]^{n-}$ Showing the Thermochemical Values That Interconvert the Cluster Congeners in MeCN[a]

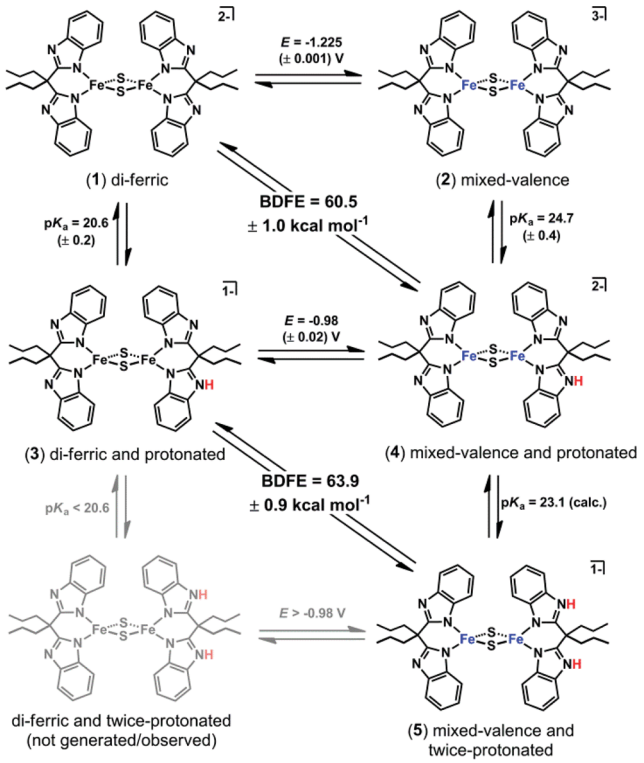

[a]The cluster shown in grey has not been observed, and the thermochemical values in grey are only estimates from other values. Potentials refer to $E_{1/2}$.

As for **4**, the twice-protonated congener **5** is NMR silent at −20 °C (5.7 mM, d_3-MeCN). Addition of 2 equiv of the strong base ^{t}BuNP (pyrr)$_3$ (pyrr = pyrrolidine) results in the reappearance of NMR resonances ascribed to **2**, in ∼75% yield, indicating reversible protonation. The EPR spectrum of **5** was obtained at 127 K (see Figure S3). The spectrum can be fit to a rhombic g tensor with g = [1.990, 1.950, 1.885] and corresponding linewidths, W = [65, 40, 60 G]. Thus, as for the other mixed-valence congeners,[15−17] **5** is S = 1/2. Though the exact site of protonation is not known (N vs S), previous studies[15] of monoprotonated **4** suggests protonation at N, and the partial localization of the electron in related systems[17,18] suggests that both protonations should occur at one iron in **5**.

II.2. Reactions of 4 and 5 with TEMPO. The reaction between **4** and the nitroxyl radical TEMPO to generate **1** and

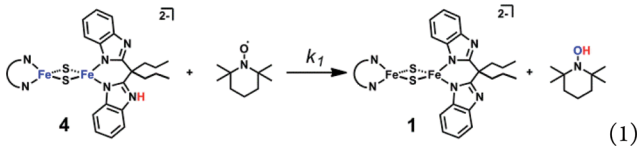

(1)

TEMPOH was previously reported (eq 1; $N^{\frown}NN$ N = ^{Pr}bbim).[15] More detailed kinetic studies on this system have now been performed using double-mixing stopped-flow kinetic measurements in MeCN under pseudo-first-order conditions of excess TEMPO. Solutions of **4** (0.25 mM) were generated in

dx.doi.org/10.1021/ic403131p | Inorg. Chem. 2014, 53, 3153−3161

situ from mixing solutions of **2** and [DMAP-H]OTf, each 0.50 mM. After a delay time of 10 s, these solutions of **4** were mixed with solutions containing excess TEMPO (~2 to 11 mM) at several temperatures (−25 to 50 °C).

To determine the KIE, solutions of **4** and *d*-**4** were generated by mixing **2** with a solution of either [DMAP-H]OTf and CH_3OH, or [DMAP-D]OTf and CD_3OD. The methanol (95 mM) was added to the acid solution to ensure high isotopic enrichment. At 25 °C, rate constants of 2480 ± 33 and 335 ± 10 M^{-1} s^{-1} were obtained for reactions of **4** and *d*-**4** with TEMPO, respectively, indicating a KIE of 7.4 ± 0.3. The k_{1H} is in agreement with that previously measured in the absence of methanol and indicates a CPET mechanism.[15] This corresponds to $\Delta G^{\ddagger}_{1H}$ = 12.8 ± 0.3 kcal mol^{-1} and $\Delta G^{\ddagger}_{1D}$ = 13.9 ± 0.3 kcal mol^{-1}. The temperature dependence of k_1 gives $\Delta S^{\ddagger}_1$ = −36.4 ± 1.4 (H) and −38.1 ± 1.6 e.u. (D), and $\Delta H^{\ddagger}_1$ = 1.99 ± 0.22 (H) and 2.62 ± 0.21 (D) kcal mol^{-1}.

To establish whether ion-pairing is affecting the kinetics of reaction 1, the room temperature measurements were repeated in 0.1 M $^{n}Bu_4NPF_6$ solutions in MeCN (**4** was generated in the absence of methanol). From these measurements, a second-order rate constant of 2750 ± 36 M^{-1} s^{-1} is obtained at 25 °C. This ~11% increase in rate upon going from 0.5 to 100 mM ionic strength is a small effect and hence ion-pairing is likely not playing a significant role.

Mixed-valence and twice-protonated **5** likewise reacts with TEMPO (eq 2) to generate diferric and protonated **3** (~ 50%)

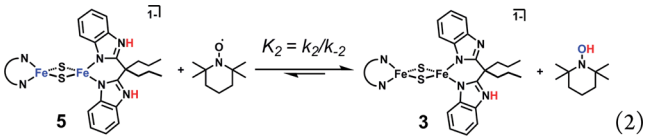

(2)

and TEMPOH (~ 100%), as ascertained by NMR spectroscopy (see Figure S22). The decreased yield of **3** relative to TEMPOH may be due to competing degradation of **5** (which likely generates paramagnetic species and free ligand, as for the degradation of **4**),[15] the instability of mixtures of **3** and **5** in the presence of TEMPOH/TEMPO, and/or the known instability of **3**.

To overcome these challenges, double-mixing stopped-flow kinetic measurements were undertaken under pseudo-first-order conditions of excess TEMPO (1.3−5.3 mM) in MeCN. Similar to the reaction described above, **5** was generated by mixing a 0.51 mM solution of **2** with a 1.01 mM solution of [DMAP-H]OTf-containing 95 mM MeOH. Optical spectra of the TEMPO reaction were consistent with cluster oxidation. However, plots of k_{obs} versus [TEMPO] have a nonzero intercept, suggesting competing degradation of **5** (k_{obs} obtained from global fitting). The kinetics were fit to a model with competing decomposition of **5**, $d[\mathbf{5}]/dt = k_{dec} + k_2[\text{TEMPO}]$. The k_{dec} values from this analysis are 0.22 ± 0.12 s^{-1} for **5** and 0.13 ± 0.02 s^{-1} for **5**-d_2 at 25 °C. The rate constants (k_2) obtained for the reactions of **5** and **5**-d_2 with TEMPO were 112 ± 30 and 30 ± 6 M^{-1} s^{-1}, respectively. This corresponds to a KIE of ~3.7. The activation free energy for the reaction of 5 with TEMPO is ~15 kcal mol^{-1} at 25 °C.

II.3. Thermochemistry of Cluster Congeners. The known thermochemical parameters that interconvert cluster congeners **1**−**4** are shown in the top portion of Scheme 1.[15] The ability to generate **5** allows construction of an expanded square scheme, in which **5** and **3** are related by PCET (Scheme 1, bottom).

The bond dissociation free energy (BDFE) of **5** was determined from the equilibrium constant for the reaction of 3 with excess TEMPOH (1.3−5.4 mM) to form **5** and TEMPO (reverse of eq 2). Owing to the instability of both **3** and **5**, K_{-2} ($K_{-2} = 1/K_2$) was determined using double-mixing stopped flow. Solutions of **3** were generated in situ from **1** and 1 equiv of [DMAP-H]OTf, and after a delay time of 1 s, then mixed with solutions containing excess TEMPOH. Upon mixing, a decrease in absorption at 526 nm was noted, indicative of cluster reduction. The resulting mixture of TEMPO, TEMPOH, **3**, and **5** is not stable, as evident from a subsequent increase in the absorption at 620 nm and loss of the isosbestic point at 350 nm (see section G of the SI). Analysis of the spectra at the inflection point of the A_{620} versus time plot, with the assumption that the equilibrium is established and degradation is limited, gives K_{-2} = 0.012 ± 0.004. A similar value of K_{-2} is obtained from spectra at later times, when degradation is known to have commenced (see section G of the SI). The K_{-2} implies a k_{-2} of 1.3 ± 0.5 M^{-1} s^{-1} and an N−H BDFE in **5** of 63.9 ± 0.9 kcal mol^{-1}, using $BDFE_{TEMPOH}$ = 66.5 kcal mol^{-1}.[19]

It is not possible to use the more typical approach to determine the N−H BDFE in **5** from the pK_a of **5** and the reduction potential of **4** (BDFE = 23.06 $E_{1/2}$ + 1.37 p*K*a + C_G; C_G = 54.9 ± 1.0 kcal mol^{-1} in MeCN).[19] The instability of **5**, coupled with the lack of NMR resonances for both **4** and **5**, prevents direct measurement of the pK_a of **5**. This equation can be used, however, to calculate the pK_a from the BDFE of **5** and the E(**3**/**4**), giving pK_a (**5**) ~ 23.1.

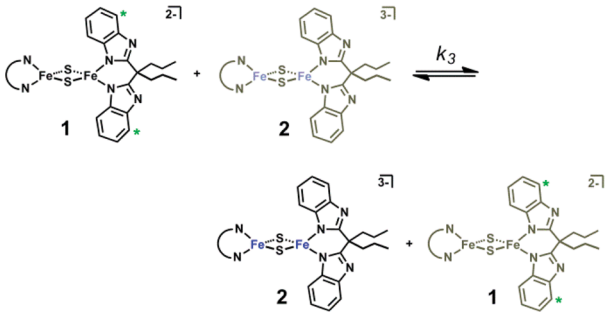

(3)

II.4. ET Self-Exchange Rates. Dynamic NMR methods were employed to determine the rate constant for intermolecular ET self-exchange between **1** and **2** (eq 3 and Figure 1). ^{1}H NMR spectra of mixtures of **1** and **2** (2.0 mM cluster, d_3-MeCN) reveal broadening of the ligand resonances of both **1** and **2**. The broadening with no change in chemical shift is indicative of slow chemical exchange on the NMR time scale.

The rate constant for intermolecular ET can be calculated from eq 4, assuming simple two-site exchange in the slow exchange limit.[20]

$$\pi\Delta W_a[a] = \pi\Delta W_b[b] = k_{self-exchange}[a][b] \quad (4)$$

In eq 4, W is the line-width at half-height for a given resonance, and $k_{self\text{-}exchange}$ is the rate constant for self-exchange between species a and b (**1** and **2** for eq 3). For this analysis, the resonance at 10.71 ppm of **1** was employed (corresponding to the 4-position of the benzimidazolate and marked with an asterisk in eq 3), as it is well-separated from the other ligand resonances of both **1** and **2**. From the slope of the plot of $\pi\Delta W_1$ versus [**2**], a value of (1.20 ± 0.06) × 10^5 M^{-1} s^{-1} is

dx.doi.org/10.1021/ic403131p | Inorg. Chem. 2014, 53, 3153−3161

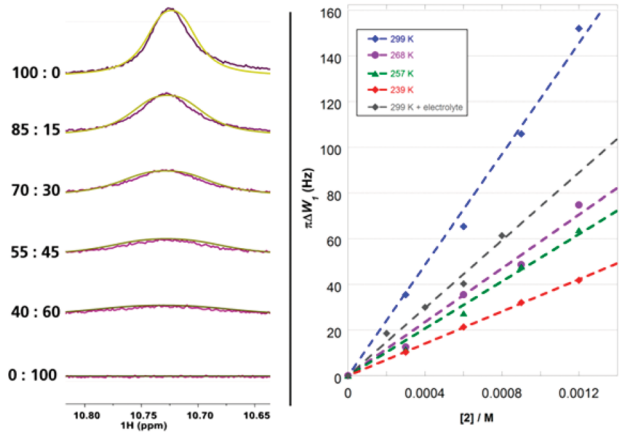

Figure 1. (Left) Overlay of stacked 1H NMR spectra (experimental: purple; fit: gold) for solutions of **1** and **2**, with [**1**] + [**2**] = 2.0 mM, in d_3-MeCN at 26 °C. The relative amounts of **1** and **2** are noted on the side. (Right) Plot of $\pi\Delta W$ (Hz) vs [**2**] (M).

obtained for k_3 at 26 °C. Analysis of the analogous resonance for **2** roughly gives the same rate constant. This corresponds to a free energy barrier of 10.5 ± 0.1 kcal mol^{-1}. Activation parameters from rate constants measured at −24, −16, −5, and 26 °C are $\Delta H^{\ddagger}_3$ = 2.2 ± 0.2 kcal mol^{-1} and $\Delta S^{\ddagger}_3$ = −28 ± 1 e.u. In the presence of 6.0 mM ^{n}Bu$_4$NPF$_6$, the rate constant is (7.4 ± 0.6) × 10^4 M^{-1} s^{-1} at 26 °C, a decrease of about 40%. This suggests ion pairing plays a role in this reaction.

The ET self-exchange rate of **3** and **4** could not be measured, owing to the high basicity of **4** (see Figure S8). Attempts to generate solutions of **3** and **4** instead results in mixtures of **1** and **5** (see Scheme 1).

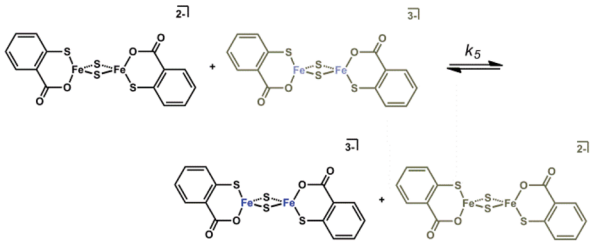

(5)

The ET self-exchange rate constant for the related [Fe$_2$S$_2$(SArO)$_2$]$^{2-/3-}$ cluster system (SArO^{2-} = thiosalicylate) was also measured by NMR line broadening (eq 5; see section F.V of the SI). For these measurements, solutions containing mixtures of the diferric and mixed-valence clusters were prepared in situ, owing to the limited stability of the mixed-valence cluster.[21] Substoichiometric amounts of CoCp*$_2$ were added to 2.5 mM solutions of [Fe$_2$S$_2$(SArO)$_2$]$^{2-}$, and then d_3-MeCN was added to adjust the final total concentration of clusters to the desired 1.9 mM. As for mixtures of **1** and **2**, ET self-exchange is slow on the NMR time scale, and eq 4 can be used to determine the rate constant. The slope of the plot of $\pi\Delta W$ versus [Fe$_2$S$_2$(SArO)$_2$]$^{2-/3-}$ (resonances for both the diferric and mixed-valence congeners were analyzed, see section F.V of the SI), indicates the rate constant k_5 = (1.9 ± 0.9) × 10^5 M^{-1} s^{-1} at 26 °C. Although the uncertainty is large, due to some scatter in the line broadening values, this rate constant is essentially the same as k_3.

II.5. PT Self-Exchange Rates. As previously reported,[15] the ^{1}H NMR spectra of both **1** and **3** have seven well-resolved ligand resonances. This indicates effective D_{2h} symmetry on the NMR time scale in solution, which requires for **3** that there be rapid proton migration among the four equivalent benzimidazolate groups. The ^{1}H NMR spectra of **1** and **3** each show a well-resolved peak for the resonance for protons at the 4-position of the benzimidazolates (marked with an asterisk in eq 6) at 10.71 and 10.65 ppm, respectively (d_3-MeCN, 25 °C).

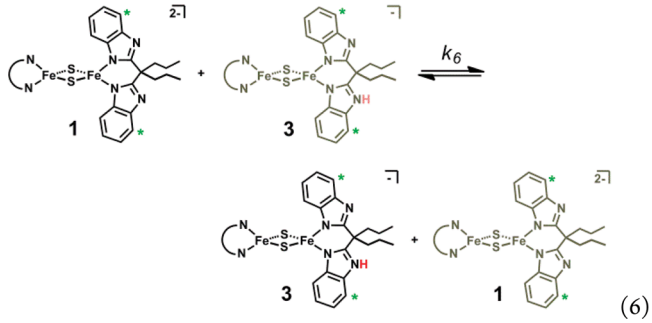

(6)

The rate of intermolecular PT exchange for **1** and **3** (eq 6) was also studied by NMR line broadening analysis. NMR spectra of mixtures of **1** and **3** in d_3-MeCN (1.94 mM; 1:3, 1:1, and 3:1) were prepared by addition of <1 equiv of [pyH]OTf to **1**. ^{1}H NMR spectra of these mixtures show a single set of ligand resonances, which shift according to the mole fraction of **1** and **3**. This indicates rapid intermolecular PT exchange between **1** and **3** on the NMR time scale. Because there is no significant broadening of the coalesced **1** + **3** signal versus the weighted average of the individual line widths, an accurate determination of the PT self-exchange rate was not possible (see Figure S5). From the peak separation, the rate constant to just achieve coalescence of the peaks[20b] would be 10^4 M^{-1} s^{-1}. This is a lower bound for k_6 at 25 °C.

The mechanism(s) for proton exchange in this system, the **1**/**3** self-exchange and the proton scrambling in **3**, are not established by these experiments. We have only succeeded in generating **3** in situ by acid addition to **1**, so the conjugate base of the acid is always present as py in the reactions described above. In addition, mixtures of **1** and **3** are not stable to excess base. Thus, we cannot determine whether the base catalyzes the proton exchanges or whether it is direct PT between clusters.

NMR line broadening analysis was also used to measure the rate constant for net intermolecular PT between the mixed-valence cluster congeners **2** and **4** (eq 7). Owing to the thermal

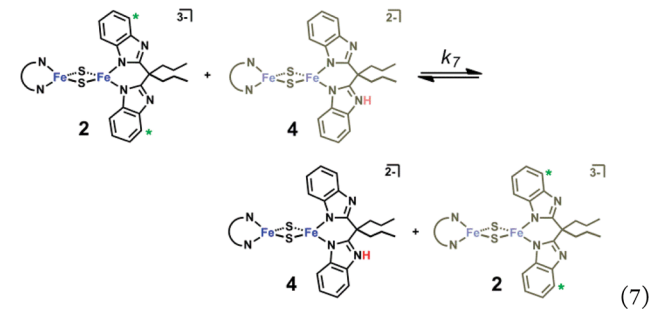

(7)

sensitivity of **4**, these measurements were done at −20 °C. As for **1**, the ^{1}H NMR spectrum of **2** (d_3-MeCN) features seven well-defined ligand resonances. By contrast, the mixed-valence and protonated congener **4** is NMR silent.[15] Addition of <1 equiv of [DMAP-H]OTf to solutions of **2** results in broadening of the resonances of **2** with no changes in the chemical shifts. This indicates that PT is slow on the NMR time scale.

dx.doi.org/10.1021/ic403131p | Inorg. Chem. 2014, 53, 3153−3161

Assuming a simple two-site exchange, the rate of intermolecular PT can be calculated from eq 4.

At −20 °C, the resonance ascribed to the protons of the 4-position in the ligand benzimidazolates is centered at 12.42 ppm and has a corresponding W_2 of 138 Hz. Upon addition of 0.2 equiv of [DMAP-H]OTf to a 5.7 mM d_3-MeCN solution of **2**, this resonance broadens to 472 Hz. This gives the rate constant k_7 of ∼9 × 10^5 M^{-1} s^{-1} at −20 °C. The peak broadens into the baseline upon addition of an additional 0.3 equiv of [DMAP-H]OTf to the sample (0.5 equiv total). As for the diferric clusters, the mechanism of PT (direct or base-mediated) is unknown.

II.6. PCET Self-Exchange Rate. The rate constant for the reaction that interconverts **1** and **4** (eq 8) was likewise obtained

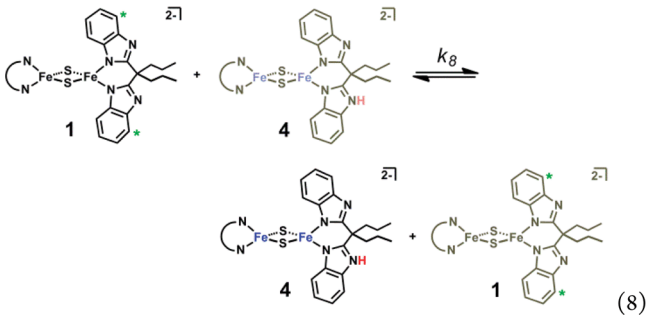

(8)

from NMR line broadening (eq 4). For these measurements, mixtures of **1** and **4** were either prepared by adding the appropriate amount of [DMAP-H]OTf to mixtures of **1** and **2** or by adding 1 equiv of [DMAP-H]OTf to a solution of **2** (to generate **4**) followed by the appropriate amount of TEMPO (see section F.VI of the SI). The same rate constant, within error, was found for both procedures (Figure 2). Peaks

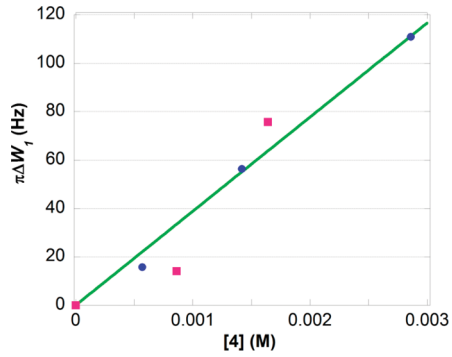

Figure 2. Plot of [**4**] (M) vs $\pi\Delta W_1$ (Hz) at −30 °C. Blue circles correspond to data collected when mixtures of **1** and **4** were prepared from mixtures of **1** and **2** + [DMAP-H]OTf. Pink squares correspond to data collected when mixtures of **1** and **4** were prepared from **4** + TEMPO. The green line is a fit to all the data.

corresponding to **1** broaden and do not shift in mixtures of **1** and **4**, showing that exchange between **1** and **4** is slow on the NMR time scale at −30 °C (**4** is NMR silent). The rate constant was obtained from the broadening of the peaks when both species were present. From the slope of the plot of $\pi\Delta W_1$ versus [**4**] (Figure 2), a value of 3.8 ± 0.7 × 10^4 M^{-1} s^{-1} is obtained for k_8 at −30 °C. This corresponds to $\Delta G^{\ddagger}_8$ = 9.0 ± 0.2 kcal mol^{-1}.

III. DISCUSSION

III.1. Comparison of Cluster Thermochemistry to Biological Rieske Clusters. The thermochemistry of interconversion between the $[Fe_2S_2(^{Pr}bbim)_x(^{Pr}bbimH_y)_{2-x}]^{n-}$ cluster congeners is shown in Scheme 1. The NH BDFE of **4** and **5** are 60.5 ± 1.0 and 63.9 ± 0.9 kcal mol^{-1}, respectively. Protonation thus modestly increases the BDFE. The twice-protonated **5** is less reducing in a PCET sense than the singly protonated **4**.

It is instructive to compare the thermochemical parameters of the model system to those of biological clusters (Table 1). *Rs*Rp and *Tt*Rp are high-potential Rieske proteins that are associated with the bc_1 complex of the Q cycle. BphF is the low potential Rieske ferredoxin of biphenyl dioxygenase, and mN is the mitoNEET cluster. The BDFEs for these clusters are obtained from the pH dependence of their aqueous reduction potentials following ref 19 (Table 1). The biologically relevant BDFEs interconvert the mono- and twice-protonated clusters, but it is valuable to see the zero/monoprotonated values as well. From this perspective, for the biologically relevant mono-protonated state, the Rieske clusters of the Q cycle are more oxidizing than either that of BphF or mN (∼6 kcal mol^{-1}) or the model cluster (∼10 kcal mol^{-1}). This is consistent with their critical role of oxidizing the appropriate hydroquinone as part of the Q cycle.[4a] By contrast, the BphF cluster serves as an ET cofactor, reducing the active-site Fe for dioxygenase enzymes.[3c]

The difference in BDFEs between the mono- and twice-protonated congeners is larger for the Q-cycle Rieske clusters (∼3.7 kcal mol^{-1}) than for the other biological clusters (∼1 kcal mol^{-1}). This may have a role in regulating the flux of e^-/H^+ in the Q cycle. A similar difference in BDFEs is observed in the model system (∼3.4 kcal mol^{-1}).

One valuable parameter for a PCET active site is the extent of *thermodynamic coupling* between the electron and the proton.[19] This is defined as the shift in pK_a upon redox change and the shift in $E_{1/2}$ upon protonation, which are equal by Hess' Law: in kcal mol^{-1}, −1.37 ΔpK_a = 23.06 $\Delta E_{1/2}$. For the unprotonated-to-monoprotonated cluster, the thermochemical coupling is 5.6 ± 0.2 kcal mol^{-1} (Table 1).[15] Because neither the reduction potential nor the pK_a of the diferric and twice-protonated cluster is known, the extent of thermochemical coupling is not known for the twice-protonated cluster. However, because the pK_a for the diferric and twice-protonated cluster must be less than that of **3**, a lower limit for the thermodynamic coupling is estimated to be 3.4 kcal mol^{-1}.

The thermodynamic coupling for the biological mono/diprotonated clusters is larger for the Rieske clusters of the Q cycle (∼6.5 kcal mol^{-1}) than for those of either BphF or mN (∼4.5 kcal mol^{-1}). The thermodynamic coupling of the model cluster in the twice-protonated state unfortunately could not be determined. The nonprotonated/monoprotonated coupling is larger for the model system (5.6 ± 0.5 kcal mol^{-1}) than for all of the biological clusters (in this protonated state). It should be noted, however, that these are all relatively small values for the PCET coupling. This coupling is ≥60 kcal mol^{-1} for TEMPOH and for toluene and can approach zero when the redox and acid/base sites are well-separated.[19]

It has been suggested that the stronger coupling in the Q-cycle clusters (relative to the oxygenase clusters) may implicate CPET, as opposed to stepwise processes.[3a] Indeed, the monoprotonated model cluster **4**, which has a similar extent

dx.doi.org/10.1021/ic403131p | *Inorg. Chem.* 2014, 53, 3153−3161

Table 1. Comparison of Thermochemical Properties for Biological and Model [2Fe−2S] Clusters

cluster	BDFE[a] (mono-/twice-protonated)	thermodynamic coupling[a] (mono-/twice-protonated)	BDFE[a] (zero-/monoprotonated)	thermodynamic coupling[a] (zero-/monoprotonated)	ref
*Rs*Rp[b,c]	75.1 ± 1.0	6.6 ± 0.6	71.5 ± 1.2	3.8 ± 0.6	3a
*Tt*Rp[b,d]	72.1 ± 1.0	6.4 ± 0.7	68.3 ± 1.7	3.5 ± 0.7	3a
BphF[b,e]	67.9 ± 1.0	4.8 ± 1.1	65.7 ± 2.2	2.5 ± 1.2	3a
mN[b,f]	67.4 ± 1.0[i]	4.1 ± 0.2	~68.2[g,i]	>3.3[h]	2b
$[Fe_2S_2(^{Pr}bbim)_2(H_x)]^{1/2/3-}$	63.9 ± 0.9	>3.4	60.5 ± 1.0	5.6 ± 0.5	15 and this work

[a]Values given in kcal mol^{-1}. Mono-/twice-protonated refers to the PCET event that interconverts the mixed-valence and twice-protonated cluster with the diferric and monoprotonated cluster. Zero-/monoprotonated refers to the PCET event that interconverts the mixed-valence and monoprotonated cluster with the diferric and deprotonated cluster. Thermodynamic coupling refers to the shift in pK_a upon redox change (and conversely the shift in $E_{1/2}$ upon protonation). [b]The BDFE and extent of thermodynamic coupling for the enzymatic clusters are calculated here from the reported reduction potentials and pK_a values (BDFE = 23.06 $E_{1/2}$ + 1.37 p*K*a + C_G; C_G = 57.6 ± 1.0 kcal mol^{-1} in water).[19] [c]*Rs*Rp = high-potential Rieske cluster from the cytochrome bc_1 complex of *Rhodobacter sphaeroides* that oxidizes ubiquinol. [d]*Tt*Rp = high-potential Rieske cluster from the cytochrome bc_1 complex of *T. Thermophilus* that oxidizes menaquinol. [e]BphF = low-potential Rieske protein that is the soluble ferredoxin of the biphenyl dioxygenase of *Burkholderia* sp. Strain LB400. [f]mN = human mitoNEET protein. [g]E_{alk}, the potential of the twice-deprotonated cluster, not reported. The sum of ΔpK_1 and ΔpK_2 must be equal to the difference between E_{alk} and E_{acid} (whcn corrected for different units). From this, E_{alk} is estimated to be ≤ −0.281 V. [h]pK_{red2} was reported as >12.5 in ref 2b. [i]Though the mitoNEET protein only has one His that coordinates the [2Fe−2S] cluster, there are two protonation events reported in ref 2b; the second protonation likely occurs at a residue near the His or cluster.

of thermodynamic coupling, is capable of undergoing concerted proton−electron transfer, as exemplified by the reaction with TEMPO, (as does **5**, vide infra). In these reactions, the preference for a CPET mechanism is largely due to the very large thermodynamic coupling of TEMPOH (~60 kcal mol^{-1}). The ability to generate the clusters that would be intermediates in the stepwise mechanism suggests that the coupling may not be substantial enough to enforce a concerted mechanism. Hence the increased coupling observed in the high-potential Rieske clusters relative to the low-potential proteins may not be sufficient to enforce a concerted mechanism. By comparison, other biological PCET cofactors have larger thermodynamic couplings: ~16.6 kcal mol^{-1} for tyrosine and ~15 kcal mol^{-1} for hydroquinone.[19] Thus, it seems that the possible mechanisms for PCET at the [2Fe−2S] clusters, concerted versus stepwise, may be determined by the extent of thermodynamic coupling in the redox partner.

III.2. Reactions with TEMPO Indicate a CPET Mechanism and a "Normal" Temperature Dependence of the KIE. The rapid H-atom transfer from **4** and **5** to TEMPO is consistent with the very low N−H BDFEs of these mixed-valence clusters. They are strong reductants (good H-atom donors). We previously reported the rate constant and activation parameters for the reaction of **4** with TEMPO (eq 1).[15] Comparison of $\Delta G^{\ddagger}_1$ with the free energy changes associated with initial ET or PT transfer, ΔG°_{ET1} and ΔG°_{PT1}, indicates that this reaction must occur via a concerted proton−electron transfer. Reported here are kinetic measurements in the presence of CH_3OH and CD_3OD to determine the kinetic isotope effect (KIE) and its temperature dependence. At 25 °C, a KIE of 7.4 ± 0.3 is observed. This corresponds to $\Delta\Delta G^{\ddagger}_{H-D}$ = −1.1 ± 0.4 kcal mol^{-1}. The entropic contributions to the activation free energy are the same (within error), and thus the difference in activation free energy is due primarily to $\Delta\Delta H^{\ddagger}_{H-D}$ = −0.63 ± 0.31 kcal mol^{-1}.

These findings are interesting in light of the unusual isotope effect observed by Cape et al. for the oxidation of ubiquinol by the cyt bc_1 complex ($\Delta E_a(D) < \Delta E_a(H)$ by 4.8 kcal mol^{-1}).[6] This effect is reproduced in other studies on quinol oxidation by a ruthenium model complex[6] and in theoretical calculations.[22] That the model system described here does not exhibit this unusual isotope effect is consistent with the idea that this effect depends on the quinol being the substrate.

The kinetic data for the reaction of **5** and TEMPO must be interpreted with caution due to the competing degradation of **5**. However, it is clear that the reaction occurs by concerted proton−electron transfer (CPET). The activation free energy of ~15 kcal mol^{-1} at 25 °C is substantially smaller than the ground state free energy changes for either initial PT or ET, $\Delta G^{\circ}_{PT} \approx 38$ kcal mol^{-1}; $\Delta G^{\circ}_{ET} > \sim 22$ kcal mol^{-1}). We simply note that the reaction is slower than that of **4** with TEMPO, 112 ± 20 M^{-1} s^{-1} for **5** versus 2480 ± 33 M^{-1} s^{-1} for **4**. This factor of ~22 lower rate constant is consistent with the lower driving force for the reaction of 5. Using the Marcus cross-relation, the 3.4 kcal mol^{-1} difference in BDFEs between **5** and **4** predicts a factor of 17 difference in rate constants, well within the uncertainties of this analysis. Thus, the CPET intrinsic barriers are not significantly different for **4** and **5**.

III.3. ET and PT Self-Exchange Rates and Implications for Biological ET Reactions. To gain further insight into the PCET reactivity of Rieske clusters, rate constants for several self-exchange processes have been measured. They are summarized in Table 2. As emphasized by Marcus, these rate constants are a direct measure of the intrinsic barrier, the intrinsic facility of the reagent to do the reaction of interest.[25]

The rate constant for ET self-exchange between **1** and **2** (eq 3) k_3 is (1.20 ± 0.06) × 10^5 M^{-1} s^{-1}. This rate constant observed is roughly 1 order of magnitude slower than that measured for related S-ligated [4Fe−4S] and [4Fe−4Se] clusters, measured analogously in d_3-MeCN at similar concentrations.[23] However, the enthalpic barrier for **1**/**2** self-exchange is ~1.4 kcal mol^{-1} *smaller* than that for $[Fe_4S_4(S\text{-}p\text{-}C_6H_4Me)_4]^{2-/3-}$. Although the differences are small, the slower ET for the [2Fe−2S] cluster system **1**/**2** is apparently due to its larger entropy of activation (by 11 e.u.) versus $[Fe_4S_4(S\text{-}p\text{-}C_6H_4Me)_4]^{2-/3-}$.

The difference in ET properties could be attributed to either the ligand type (N vs S) and/or the cluster size. To distinguish between these possibilities, the ET self-exchange rate for a second type of [2Fe−2S] cluster was sought. The instability of S-ligated mixed-valence [2Fe−2S] clusters precluded a direct comparison of all S-ligated clusters,[26] so instead, the mixed S/O-ligated cluster, $[Fe_2S_2(SArO)_2]^{2-/3-}$ was examined. The ET self-exchange rate constant k_5 for this cluster (eq 5) is (1.9 ± 0.9) × 10^5, which is within the uncertainty of the value for **1**/**2**

dx.doi.org/10.1021/ic403131p | Inorg. Chem. 2014, 53, 3153−3161

Table 2. Kinetic Data for Self-Exchange Reactions of Bis-Benzimidazolate Ligated [2Fe−2S] Clusters and Related Systems

reaction	type	k (M^{-1} s^{-1})	$\Delta G^{‡}$ (kcal mol^{-1})	$\Delta H^{‡}$ (kcal mol^{-1})	$\Delta S^{‡}$ (cal K^{-1} mol^{-1})	ref
[a] **1** + **2**	ET	1.20 (±0.06) × 10^5	10.5 (±0.1)	2.2 (±0.2)	−28 (±1)	this work
[b] **1** + **2**	ET	7.4 (±0.6) × 10^4				this work
[c,j] **1** + **3**	PT	[j] >10^4				this work
[d,k] **2** + **4**	PT	[k] ~9 × 10^5				this work
[e,k] **1** + **4**	CPET	3.8 (±0.7) × 10^4	9.0 (±0.1)			this work
[a] $[Fe_2S_2(SArO)_2]^{2-/3-}$	ET	1.9 (±0.9) × 10^5	10.3 (±0.3)			this work
[f] $[Fe_4S_4(SCH_2Ph)_4]^{2-/3-}$	ET	2.4 (±0.2) × 10^6				23
[g] $[Fe_4S_4(S\text{-}p\text{-}C_6H_4Me)_4]^{2-/3-}$	ET	2.8 (±0.3) × 10^6	8.7	3.6	−17	23
[h] $[Fe_4Se_4(S\text{-}p\text{-}C_6H_4Me)_4]^{2-/3-}$	ET	9.7 (±0.9) × 10^6				23
[i] $[Fe(H_2bim)_3]^{2+/3+}$	ET	1.7 (±0.2) × 10^4	11.7 (±0.2)	4.1 (±0.3)	−25 (±1)	24
[c,i] $[Fe^{III}(H_2bim)_2(Hbim)]^{2+}$ + $[Fe^{III}(H_2bim)_3]^{3+}$	PT	~2 × 10^6	9 (±1)			24
[c,i] $[Fe^{III}(H_2bim)_2(Hbim)]^{2+}$ + $[Fe^{II}(H_2bim)_3]^{2+}$	CPET	5.8 (±0.6) × 10^3	12.3 (±0.2)	4.4 (±0.7)	−26 (±2)	24

[a]Measured at 299 K in d_3-MeCN. [b]Measured at 299 K in d_3-MeCN with 6.0 mM $^nBu_4NPF_6$. [c]Measured at 298 K in d_3-MeCN. [d]Measured at 253 K in d_3-MeCN. [e]Measured at 243 K in d_3-MeCN. [f]Measured at 300 K in d_3-MeCN. [g]Measured at 301 K in d_3-MeCN. [h]Measured at 304 K in d_3-MeCN. [i]H_2bim = 2,2′-bi-imidazoline. [j]Measured in the presence of pyridine (equimolar with **3**). [k]Measured in the presence of DMAP (equimolar with **4**).

and again roughly an order of magnitude slower than that of the related [4Fe−4S] clusters.

The effect of cluster size on high-spin iron species can be further examined by contrasting the ET self-exchange rates of the [2Fe−2S] clusters to $[Fe(H_2bim)_3]^{2+/3+}$ monomeric complexes. The ET self-exchange rates for the [2Fe−2S] clusters are ~1 order of magnitude larger than in the monomeric systems.[24] Thus, our results suggest that cluster size, not ligand composition, controls the ET self-exchange kinetics for high-spin iron species. The larger clusters have larger ET self-exchange rates and smaller intrinsic barriers. This may be attributed to more electron delocalization as cluster size increases, which would decrease both the inner- and outer-sphere reorganization energies.

The self-exchange rate constants reflect the intrinsic barriers and therefore the rate of all ET reactions involving these reagents, following Marcus theory. The differences highlighted here should correspond to a factor of 3−4 times in cross rate constants ([4Fe−4S] vs [2Fe−2S], or [2Fe−2S] vs [Fe]), for ET reactions with different redox partners. These results clearly indicate that the cluster size modulates the intrinsic barrier to ET. This contrasts with previous computational studies that predicted no clear trend for the inner-sphere reorganization energy of [Fe−S] clusters with size (in vacuum).[27] These studies do however suggest that the hydrogen-bonding of the protein environment can substantially reduce the inner-sphere reorganization energy. Comparison of self-exchange rates of synthetic and biological [4Fe−4S] clusters indicate a much slower self-exchange rate for biological clusters.[23,28] Combined, this underscores the importance of hydrogen bonds,[27,29] sterics, and the local protein environment to reorganization energies. Nonetheless, for proteins with similar environments, the results presented here suggest that the rate of ET should vary with cluster size.

The control of ET rates to/from enzyme active-sites is crucial for catalysis. Nature employs a variety of [FeS] clusters which differ in size, ligand, and metal identity, and the choice of cluster type remains unknown. It has been proposed that the choice of cluster may be in part due to stability[1a] and/or redox potential.[27] Computational studies suggest that [4Fe−4S] clusters are more robust than smaller analogues upon metal substitution,[30] maintaining similar inner-sphere reorganization energies and hence ET rates. The results presented here indicate that the cluster size also contributes the rate of ET and hence may also contribute to the choice of cluster in proteins.

Interpretation of the PT rate constants must be done with caution, as the presence of the conjugate base of the acid used to protonate the cluster is present in solution. We simply note that in the presence of the conjugate base, the PT self-exchange rate constants are faster than the ET ones. The values obtained are similar to that of the related monomeric $[Fe(H_2bim)_3]^{3+}$ analogue (obtained in the absence of the conjugate base).[24]

Albers et al. recently showed that for a related bis-benzimidazolate ligated [2Fe−2S] cluster,[17] electron localization increases upon protonation in the mixed-valence state. This suggests that the change in electron localization (which would increase both inner- and outer-sphere reorganization energies) might affect PT. Unfortunately, owing to the difficulties in obtaining accurate PT rate constants for the system, no conclusions can be drawn from our PT studies.

III.4. PCET Self-Exchange Rates and Implications for Rieske and mitoNEET Clusters. The rate constant for net PCET self-exchange between **1** and **4** is (3.8 ± 0.7) × 10^4 M^{-1} s^{-1} at −30 °C. This is slower than the PT and ET self-exchange rates, by ~2 and 1 orders of magnitude, respectively. This self-exchange reaction could occur via concerted transfer of e^- and H^+ or by a stepwise ET-PT or PT-ET path. Initial ET and PT have different transition states and barrier heights, but for the special case of a self-exchange reaction, they yield the same intermediates (eq 9).[24] Additionally, for a self-exchange process, the overall ET-PT and PT-ET paths are the microscopic reverse of each other (eqs 9 and 10). They must therefore proceed at the same overall rate for this $\Delta G^{\circ} = 0$ process.

The equilibrium constant K_9 for eq 9 is ~8 × 10^{-5}, based on the difference in pK_a values of **3** and **4** (equal to the difference in $E_{1/2}$ of **1** and **3**; this is equal to the thermochemical coupling).

$$\mathbf{1} + \mathbf{4} \xrightarrow{\text{PT or ET}} \mathbf{2} + \mathbf{3} \quad (9)$$

$$\mathbf{2} + \mathbf{3} \xrightarrow{\text{ET or PT}} \mathbf{1} + \mathbf{4} \quad (10)$$

The reverse of eq 9, **2** + **3** (eq 10), cannot occur faster than the diffusion limit in MeCN, $k_{-9} \leq 2 \times 10^{10}$ M^{-1} s^{-1}.[31] As $K_9 = k_9/k_{-9}$, k_9 must be less than ~10^6 M^{-1} s^{-1}. Thus, the stepwise

dx.doi.org/10.1021/ic403131p | Inorg. Chem. 2014, 53, 3153−3161

mechanism of initial ET or PT is potentially kinetically competent.

The rate constant for initial ET can be estimated from the Marcus cross-relation (eq 11).[25]

$$k_{xy} = \sqrt{k_{xx}k_{yy}K_{xy}f_{xy}} \quad (11)$$

In eq 11, k_{xy} is the rate constant for the ET cross reaction of 1 with **4**, k_{xx} and k_{yy} are the self-exchange rate constants for **1**/**2** and **3**/**4**, respectively, and K_{xy} is the equilibrium constant for the cross reaction. f_{xy} is a known function of k_{xy}, k_{xx}, k_{yy}, and the individual work terms associated with formation of the precursor/successor complexes of the cross- and self-exchange reactions. Assuming that $k_{3/4}$ can be approximated as $\approx k_{1/2}$ ($\sim 2 \times 10^3$ M^{-1} s^{-1} at 243 K), and that $K_{1/4}$ has no temperature dependence, then $k_{1/4}$ is predicted to be ~ 20 M^{-1} s^{-1} ($f \sim 1$). This corresponds to $\Delta G^{\ddagger} \sim 13$ kcal mol^{-1} for initial ET. This argues against a stepwise ET-PT mechanism for the PCET process, because this ET barrier is ~ 4 kcal mol^{-1} larger than the measured activation free energy for the PCET self-exchange of **1** and **4**. As the overall ET-PT and PT-ET paths are the microscopic reverse of one another, this also argues against the PT-ET mechanism (Figure 3).

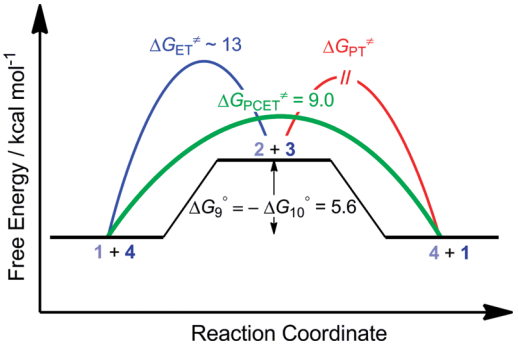

Figure 3. Free energy diagram for the PCET self-exchange reaction of **1** and **4**. The peak of the green (lowest) curve is the measured PCET barrier. The blue and red curves represent the stepwise ET-PT mechanism, with the height of the ET step (blue) derived from the Marcus Cross relation (eq 11). The magnitude of the PT barrier is not known. The PT-ET mechanism is the microscopic reverse (red then blue).

To establish the feasibility of a CPET mechanism, the Marcus cross-relation can again be utilized. We have shown that the Marcus cross-relation (eq 11) can be used to predict rate constants for CPET cross reactions within 1−2 orders of magnitude.[32] From the Eyring equation, the rate constant for PCET self-exchange between **1** and **4** at 25 °C is estimated to be $\sim 1.5 \times 10^6$ M^{-1} s^{-1}. The self-exchange rate constant for TEMPO/TEMPOH in MeCN is 4.7 M^{-1} s^{-1},[33] and the equilibrium constant for the reaction of **4** with TEMPO is 2.5×10^4. From these values, the Marcus cross-relation predicts the rate constant of 3.0×10^5 M^{-1} s^{-1} for the reaction of **4** with TEMPO ($f \sim 0.5$). The measured cross rate constant of 2480 ± 33 M^{-1} s^{-1} is ~ 2 orders of magnitude slower than that predicted from the Marcus cross-relation. Thus, these results are consistent with the measured PCET self-exchange rate constant for **1**/**4** corresponding to a CPET pathway. Additionally, these results suggest that the cross-relation can be applied to CPET reactions that involve [Fe−S] clusters and hence can be more broadly applied to biological systems and related clusters that do not have localized valences.

Thus, the mechanism for PCET self-exchange between **1** and **4** likely occurs via a CPET mechanism. The ΔG° to form the intermediates of the stepwise mechanism—the thermochemical coupling of ~ 5.6 kcal mol^{-1}—is high enough to preclude the stepwise mechanism, but not by much. This choice of mechanisms is also likely important for biological Rieske clusters, which have a similar extent of thermodynamic coupling.

IV. CONCLUSIONS

This report describes the PCET reactivity and thermochemistry of a set of bis-benzimidazolate-ligated [2Fe−2S] clusters. PCET can occur from two distinct protonation states, between complexes **1** and **4** or between **3** and **5**. The measured ET self-exchange rate constants for **1**/**2** and for the related [2Fe−2S] cluster $[Fe_2S_2(SArO)_2]^{2-/3-}$ are both an order of magnitude slower than that of the larger S-ligated [4Fe−4S] clusters. ET self-exchange for the [2Fe−2S] clusters is an order of magnitude faster than that of a related high-spin mononuclear iron complex, suggesting that the intrinsic barrier to ET is modulated by cluster size. The measured rate constant for PCET self-exchange between **1** and **4** is consistent with a CPET mechanism. Combined, these findings suggest a small bias for CPET mechanisms at imidazole-ligated [2Fe−2S] clusters such as the Rieske and mitoNEET clusters. However, the choice of mechanism—stepwise versus concerted—is likely controlled by the thermodynamic coupling of the redox partner.

■ ASSOCIATED CONTENT

Ⓢ Supporting Information

Experimental procedures, characterization of **5**, exemplary kinetics data and plots (.pdf). This material is available free of charge via the Internet at http://pubs.acs.org.

■ AUTHOR INFORMATION

Corresponding Author

*E-mail: mayer@chem.washington.edu.

Present Address

‡Department of Chemistry, University of Utah, 315 South 1400 East, Salt Lake City, Utah 84112, U.S.A.

Notes

The authors declare no competing financial interest.

■ ACKNOWLEDGMENTS

The authors gratefully acknowledge the U.S. National Institutes of Health, GM50422 to J.M. and 1F32GM099316 to C.S., and a Levinson Scholar Award to M.P., for financial support.

■ REFERENCES

(1) (a) Beinert, H.; Holm, R. H.; Münck, E. *Science* **1997**, *277*, 653. (b) Lippard, S. J.; Berg, J. M. *Principles of Bioinorganic Chemistry*; University Science Books: Mill Valley, CA, 1994.

(2) (a) Zu, Y.; Fee, J. A.; Hirst, J. *J. Am. Chem. Soc.* **2001**, *123*, 9906. (b) Bak, D. W.; Zuris, J. A.; Paddock, M. L.; Jennings, P. A.; Elliott, S. J. *Biochemistry* **2009**, *48*, 10193. (c) Camba, R.; Jung, Y.-S.; Hunsicker-Wang, L. M.; Burgess, B. K.; Stout, C. D.; Hirst, J.; Armstrong, F. A. *Biochemistry* **2003**, *42*, 10589. (d) Lanzilotta, W. N.; Christiansen, J.; Dean, D. R.; Seefeldt, L. C. *Biochemistry* **1998**, *37*, 11376.

(3) (a) Zu, Y.; Couture, M. M. J.; Kolling, D. R. J.; Crofts, A. R.; Eltis, L. D.; Fee, J. A.; Hirst, J. *Biochemistry* **2003**, *42*, 12400. (b) Hsueh, K.-

L.; Westler, W. M.; Markley, J. L. *J. Am. Chem. Soc.* **2010**, *132*, 7908. (c) Ferraro, D. J.; Gakhar, L.; Ramaswamy, S. *Biochem. Biophys. Res. Commun.* **2005**, *338*, 175.
(4) (a) Osyczka, A.; Moser, C. C.; Dutton, P. L. *Trends Biochem. Sci.* **2005**, *30*, 176. (b) Berry, E. A.; Guergova-Kuras, M.; Huang, L.-S.; Crofts, A. R. *Annu. Rev. Biochem.* **2000**, *69*, 1005.
(5) Lhee, S.; Kolling, D. R. J.; Nair, S. K.; Dikanov, S. A.; Crofts, A. R. *J. Biol. Chem.* **2010**, *285*, 9233.
(6) Cape, J. L.; Bowman, M. K.; Kramer, D. M. *J. Am. Chem. Soc.* **2005**, *127*, 4208.
(7) (a) Cape, J. L.; Aidasani, D.; Kramer, D. M.; Bowman, M. K. *Biochemistry* **2009**, *48*, 10716. (b) Cape, J. L.; Bowman, M. K.; Kramer, D. M. *Proc. Natl. Acad. Sci. U.S.A.* **2007**, *104*, 7887.
(8) Paddock, M. L.; Wiley, S. E.; Axelrod, H. L.; Cohen, A. E.; Roy, M.; Abresch, E. C.; Capraro, D.; Murphy, A. N.; Nechushtai, R.; Dixon, J. E.; Jennings, P. A. *Proc. Natl. Acad. Sci. U.S.A.* **2007**, *104*, 14342.
(9) Kusminski, C. M.; Holland, W. L.; Sun, K.; Park, J.; Spurgin, S. B.; Lin, Y.; Askew, G. R.; Simcox, J. A.; McClain, D. A.; Li, C.; Scherer, P. E. *Nat. Med.* **2012**, *18*, 1539.
(10) Sohn, Y.-S.; Tamir, S.; Song, L.; Michaeli, D.; Matouk, I.; Conlan, A. R.; Harir, Y.; Holt, S. H.; Shulaev, V.; Paddock, M. L.; Hochberg, A.; Cabanchick, I. Z.; Onuchic, J. N.; Jennings, P. A.; Nechushtai, R.; Mittler, R. *Proc. Natl. Acad. Sci. U.S.A.* **2013**, *110*, 14676.
(11) Zuris, J. A.; Harir, Y.; Conlan, A. R.; Shvartsman, M.; Michaeli, D.; Tamir, S.; Paddock, M. L.; Onuchic, J. N.; Mittler, R.; Cabantchik, Z. I.; Jennings, P. A.; Nechushtai, R. *Proc. Natl. Acad. Sci. U.S.A.* **2011**, *108*, 13047.
(12) Wiley, S. E.; Paddock, M. L.; Abresch, E. C.; Gross, L.; van der Geer, P.; Nechushtai, R.; Murphy, A. N.; Jennings, P. A.; Dixon, J. E. *J. Biol. Chem.* **2007**, *282*, 23745.
(13) Bak, D. W.; Elliott, S. J. *Biochemistry* **2013**, *52*, 4687.
(14) Zuris, J. A.; Halim, D. A.; Conlan, A. R.; Abresch, E. C.; Nechushtai, R.; Paddock, M. L.; Jennings, P. A. *J. Am. Chem. Soc.* **2010**, *132*, 13120.
(15) Saouma, C. T.; Kaminsky, W.; Mayer, J. M. *J. Am. Chem. Soc.* **2012**, *134*, 7293.
(16) (a) Albers, A.; Demeshko, S.; Dechert, S.; Bill, E.; Bothe, E.; Meyer, F. *Angew. Chem., Int. Ed.* **2011**, *50*, 9191. (b) Beardwood, P.; Gibson, J. F. *J. Chem. Soc., Dalton Trans.* **1992**, 2457.
(17) (a) Albers, A.; Bayer, T.; Demeshko, S.; Dechert, S.; Meyer, F. *Chem.—Eur. J.* **2013**, *19*, 10101. (b) Added in proof: See also: Albers, A.; Demeshko, S.; Dechert, S.; Saouma, C. T.; Mayer, J. M.; Meyer, F. *J. Am. Chem. Soc.* **2014**, DOI: 10.1021/ja412449v.
(18) (a) Ballmann, J.; Albers, A.; Demeshko, S.; Dechert, S.; Bill, E.; Bothe, E.; Ryde, U.; Meyer, F. *Angew. Chem., Int. Ed.* **2008**, *47*, 9537. (b) Ding, X. Q.; Bill, E.; Trautwein, A. X.; Winkler, H.; Kostikas, A.; Papaefthymiou, V.; Simopoulos, A.; Beardwood, P.; Gibson, J. F. *J. Chem. Phys.* **1993**, *99*, 6421.
(19) Warren, J. J.; Tronic, T. A.; Mayer, J. M. *Chem. Rev.* **2010**, *110*, 6961.
(20) (a) Sowrey, F. E.; MacDonald, C. J.; Cannon, R. D. *J. Chem. Soc., Faraday Trans.* **1998**, *94*, 1571. (b) Sandström, J. *Dynamic NMR Spectroscopy*. Academic Press, Inc.: New York, 1982.
(21) Saouma, C. T.; Kaminsky, W.; Mayer, J. M. *Polyhedron* **2013**, *58*, 60.
(22) Ludlow, M. K.; Soudackov, A. V.; Hammes-Schiffer, S. *J. Am. Chem. Soc.* **2009**, *131*, 7094.
(23) Reynolds, J. G.; Coyle, C. L.; Holm, R. H. *J. Am. Chem. Soc.* **1980**, *102*, 4350.
(24) Roth, J. P.; Lovell, S.; Mayer, J. M. *J. Am. Chem. Soc.* **2000**, *122*, 5486.
(25) Marcus, R. A.; Sutin, N. *Biochim. Biophys. Acta, Rev. Bioenerg.* **1985**, *811*, 265.
(26) Venkateswara Rao, P.; Holm, R. H. *Chem. Rev.* **2004**, *104*, 527.
(27) Sigfridsson, E.; Olsson, M. H. M.; Ryde, U. *Inorg. Chem.* **2001**, *40*, 2509.
(28) (a) Cummins, D.; Gray, H. B. *J. Am. Chem. Soc.* **1977**, *99*, 5158. (b) Rawlings, J.; Wherland, S.; Gray, H. B. *J. Am. Chem. Soc.* **1977**, *99*, 1968.
(29) Dey, A.; Jenney, F. E.; Adams, M. W. W.; Babini, E.; Takahashi, Y.; Fukuyama, K.; Hodgson, K. O.; Hedman, B.; Solomon, E. I. *Science* **2007**, *318*, 1464.
(30) (a) Jensen, K. P.; Ooi, B.-L.; Christensen, H. E. M. *J. Phys. Chem. A* **2008**, *112*, 12829. (b) Jensen, K. P. *J. Inorg. Biochem.* **2006**, *100*, 1436.
(31) Grampp, G.; Jaenicke, W. *Ber. Bunsen-Ges. Phys. Chem.* **1991**, *95*, 904.
(32) Mayer, J. M. *Acc. Chem. Res.* **2011**, *44*, 36.
(33) Mader, E. A.; Larsen, A. S.; Mayer, J. M. *J. Am. Chem. Soc.* **2004**, *126*, 8066.